Measurement of A_{nn}, A_{no}, and A_{on} for the reaction $pp \rightarrow d\pi^+$ in the energy region 500–800 MeV

W. B. Tippens,* T. S. Bhatia,† G. Glass, J. C. Hiebert, R. A. Kenefick, and L. C. Northcliffe
Texas A&M University, College Station, Texas 77843

J. G. J. Boissevain, J. J. Jarmer, and J. E. Simmons
Los Alamos National Laboratory, Los Alamos, New Mexico 87545

D. H. Fitzgerald,† J. Holt,‡ and A. Mokhtari§
University of California, Los Angeles, California 90024

G. E. Tripard
Washington State University, Pullman, Washington 99164
(Received 6 April 1987)

Angular distributions of the spin observables A_{nn}, A_{no}, and A_{on} for the reaction $pp \rightarrow d\pi^+$ have been measured for pion c.m. angles $30° < \theta_\pi^* < 110°$ at beam kinetic energies of 500, 600, 650, 700, 733, and 800 MeV. These are precision data spanning the energy region of two conjectured dibaryon resonances in the NN system, one near 650 MeV ($^1D_2$) and one near 750 MeV ($^3F_3$). The A_{nn} data have significant impact on the partial-wave analyses and are in disagreement with the predictions of existing models. The data show no direct evidence for the existence of either of the two dibaryon resonances.

I. INTRODUCTION

The reaction $pp \rightleftarrows d\pi^+$ has been studied for the past 30 years because of its importance to the understanding of pion production and absorption in nuclei. It is also important in that, having two-body initial and final states, it is the simplest reaction to study involving three-body dynamics. Speculation on the existence of dibaryon resonances in the NN system and recognition of the importance of the coupling between the pion-production channel and the elastic π and NN channels has increased the interest in this reaction in recent years. Early theoretical work showed that the differential cross section is dominated by the Δ isobar.[1–4] In the energy region of the present experiment the Δ resonance contributes primarily through the singlet amplitudes, which largely determine the differential cross section, both in shape and magnitude. Spin dependence, however, is likely to be more sensitive to a combination of singlet and triplet amplitudes, and because the early models did not treat the dynamics of the triplet amplitudes correctly, their predictions did not agree with early polarization data.

More recently, theorists have been trying to improve their understanding of the three-body dynamics of the reaction. Various coupled-channel models have been developed based on separable or local potentials.[5–11] The most advanced of these use Faddeev equations to couple in momentum space. They maintain three-body unitarity but are not completely relativistic, which may be one reason why they do not accurately describe the spin-observable data above 600 MeV. Recently, Locher and Švarc attempted a calculation using relativistic perturbation theory to estimate the dominant pion rescattering term. However, only when they add some *ad hoc* modifications do their predictions begin to fit the data.

Since, to some extent, these theories are phenomenological, they require input information from existing data. In particular, precision spin-observable data are needed to define the six complex scattering amplitudes of the reaction more precisely, thus aiding in discrimination between the different approaches to the three-body dynamics. In addition to the uncertainties in the dynamics, there is the question of the possible existence of inelastic dibaryon resonances in the NN system. If they do exist, their effects would be expected in the inelastic channels, including the $NN \rightarrow d\pi$ reaction. Some efforts have been made to see whether dibaryons are inferred by the MIT quark bag model.[13,14] Most of the evidence for their existence comes from observed structure in the pp polarized total cross sections,[15] structure in πd elastic scattering,[16,17] and the evidence for poles in the S matrix found in partial-wave or phase-shift analyses.[18,19] Alternatively, these "resonance" effects could be due instead to dynamics of the reaction not involving dibaryon resonances.[11,20–23] Obviously, more precise and complete data for the polarization observables[24] are needed in order to develop more accurate reaction models before these questions can be dealt with properly. Prior to the present experiment, which has been partially reported earlier,[25] the only data available in this energy region were angular distributions of the differential cross section and analyzing power,[26–33] and some spin correlation data between 500 and 600 MeV.[34–36] Precision

analyzing-power measurements were made by an independent group[37] while the present experiment was in progress. In a companion to the present experiment, the spin-correlation parameters A_{ll} and A_{sl} were also measured over this energy region.[38] Laptev and Strakovsky[39] have compiled a collection of data available on the $pp \rightarrow d\pi^+$ reaction up to 1984.

There are six independent complex amplitudes that uniquely describe the $pp \rightarrow d\pi$ reaction. In the notation of Foroughi,[24] they are S, M_1, M_4, T_2, T_3, and T_6. The singlet amplitude S is the result of pp singlet initial waves only, while T_2, T_3, and T_6 are triplet amplitudes that result only from pp triplet initial waves, and M_1 and M_4 are mixed amplitudes that are the result of both singlet and triplet initial waves. The mixed amplitudes M_1 and M_4 can be combined to form purely singlet (M_s) and triplet (M_t) amplitudes:

$$M_s = M_1 - M_4, \quad M_t = M_1 + M_4 \ . \tag{1}$$

Locher and Švarc[12] have shown that M_1 and M_4 are approximately equal and opposite in sign over the entire angular distribution at the energies of interest to this experiment, and that this result is due to the dominance of the Δ isobar. This near equality is also expected since M_s is expected to be large and M_t to be small in this energy region. The amplitudes T_2 and T_3 are related by the symmetry $T_2(\theta_\pi^*) = -T_3(\pi - \theta_\pi^*)$. The unpolarized differential cross section is given by

$$\sigma_{00} = \tfrac{1}{2}(|S|^2 + |M_1|^2 + |M_4|^2 + |T_2|^2 + |T_3|^2 + |T_6|^2) \ . \tag{2}$$

If M_1 and M_4 are replaced by their expressions in terms of M_s and M_t, no interference occurs between singlet and triplet amplitudes in σ_{00}. In the absence of this interference, the large singlet terms dominate the unpolarized cross section and very little structure is evident in σ_{00}. The angular dependence of σ_{00} is smooth, with a $\cos^2\theta_\pi^*$ and a small $\cos^4\theta_\pi^*$ dependence.

The analyzing power,

$$A_{no} = \frac{1}{P_b} \frac{\sigma\uparrow - \sigma\downarrow}{\sigma\uparrow + \sigma\downarrow}$$

(where P_b is the beam polarization and the arrows indicate its sign), can be expressed in terms of these amplitudes as

$$A_{no} = (\sigma_{00})^{-1} \mathrm{Im}(M_1 T_3^* - M_4 T_2^* + S T_6^*) \ , \tag{3}$$

which shows that the structure in A_{no} is primarily due to interference between the small and poorly known triplet amplitudes and the larger singlet amplitudes. In the orthogonal geometry ($\theta_\pi^* = 90°$) both M amplitudes vanish, leaving only the ST_6^* term, which gives information on the interference between S and T_6.

The spin correlation parameter A_{nn} is given by

$$A_{nn} = -1 + (2\sigma_{00})^{-1}(|M_t|^2 + |T_2 - T_3|^2) \ , \tag{4}$$

where the double subscript indicates normal polarization of both beam and target. Clearly, any deviation from -1 is a result of nonzero triplet contributions to the reaction. Since the M_t term is very small at all angles the deviation in A_{nn} from -1 must be due to the T amplitudes. Since $T_2 = -T_3$ and $M_t = 0$ in the orthogonal geometry, then

$$\frac{2}{\sigma_{00}} |T_2|^2 = 1 + A_{nn} \ , \tag{5}$$

and the magnitude of T_2 at $\theta_\pi^* = 90°$ is entirely determined by a measurement of A_{nn}. The experimental definition of A_{nn} for beam and target polarization, P_b and P_t, respectively, is

$$A_{nn} = \frac{1}{P_b P_t} \frac{(\sigma\uparrow\uparrow + \sigma\downarrow\downarrow) - (\sigma\uparrow\downarrow + \sigma\downarrow\uparrow)}{(\sigma\uparrow\uparrow + \sigma\downarrow\downarrow + \sigma\uparrow\downarrow + \sigma\downarrow\uparrow)} \ ,$$

where the arrows indicate the up and down directions of the beam and target polarizations with respect to the normal to the scattering plane.

II. EXPERIMENTAL METHOD AND APPARATUS

The experiment was done at the Clinton P. Anderson Meson Physics Facility (LAMPF) with a vertically polarized proton beam and a vertically polarized hydrogen target (PPT). A schematic drawing of the experimental apparatus is shown in Fig. 1. The deuteron from the reaction was detected in a magnetic spectrometer. The pion in coincidence was detected in a recoil counter array at the conjugate angle. The measured quantity was the scattering asymmetry for a given angle under reversal of the beam polarization (every minute) and target polarization (every few hours).

A. Beam monitoring

The shape and position of the polarized beam were monitored by two profile monitors (PM1, PM2). The beam was focused on target by two quadrupole magnets (QM1, QM2) and centered on the target by two steering magnets (SM1, SM2). Steering of the beam had to be changed for each beam energy due to the varying deflection of the beam by the polarized proton target (PPT) magnet. The profile monitors could not be used for the initial centering of the beam on target because of the deflection of the beam by the PPT magnet. Verification of beam centering was done by taking double-exposure polaroid photographs of the target with the beam both focused and defocused, providing an image of the target with the beam spot superimposed.

The primary beam current monitor was an integrating

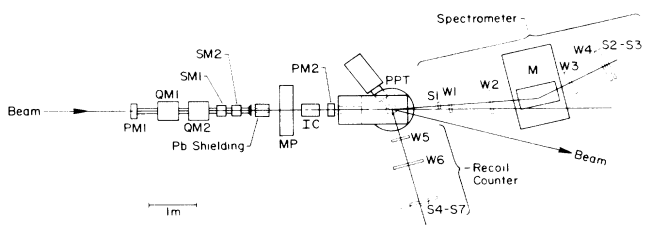

FIG. 1. Layout of the experimental setup.

ion chamber (IC) that generated a dc output current proportional to the beam current passing through it. Typical average beam currents during data runs were from 0.5–1.5 pA.

The scaled integrated IC output was used to determine the length of data runs and to normalize for run-to-run differences of integrated beam current. It was also used to measure the magnitude of the beam polarization using the quench-ratio method, as will be described in Sec. III C. The temperature and pressure of the IC were monitored throughout the experiment, since changes in these parameters would cause a change in the calibration of the chamber.

The vector polarization of the beam was observed with a monitor polarimeter (MP) system that consisted of two double-arm polarimeters. One arm measured a left-right scattering asymmetry to determine the amount of beam polarization in the vertical (y) direction, while the other measured an up-down scattering asymmetry to determine the amount of polarization in the horizontal (x) direction. Figure 2 shows the geometry for both polarimeters. Each arm consisted of two plastic scintillator detectors that detected both protons from elastic pp scattering near 17° lab from a CH_2 target of 1.6 mm thickness. The large solid-angle acceptance ($\sim$40 msr) of each polarimeter allowed a significant proportion of the signal to be p-C quasielastic scattering. No attempt was made to correct for this contamination; instead, the polarimeters were calibrated empirically by the quench-ratio method using the ion chamber data. The calibration procedure is described in Sec. III C. Typical rates for each arm were 20–40 kHz/pA with an accidental rate of $\sim$5%. Average beam polarization was $\sim$70% and gave asymmetries of $\sim$0.25 in the polarimeters.

B. Polarized target

Propanediol (CH_3-CHOH-CH_2OH) was the target material. This material, in the form of spherical beads about 1 mm in diameter, filled the target cell, which was a cylindrical microwave cavity of diameter 2 cm and length 4 cm (volume: 12.6 cm^3), formed from a copper sheet of 0.12 mm thickness with a liner of Teflon of 0.12 mm thickness. The cylindrical axis of the target was horizontal, oriented at an angle of 60° to the incident beam direction. The absolute hydrogenic density of the target material was $\sim$0.07 g/cm^3. The target material was cooled by a ^{3}He refrigeration system to a temperature of about 0.5 K. An external field of 2.5 T was supplied by a conventional water-cooled magnet (PTM) with a "C" yoke, with pole pieces specially shaped to supply an extremely uniform ($\sim\pm$5G) vertical field over the target volume. The beam entered the target through a 13 cm diam hole in the magnet yoke. The target was dynamically polarized to typically 80% throughout the experiment. The polarization was monitored every three minutes during data runs using a new nuclear magnetic resonance (NMR) technique[40] that removed the dispersive component of the NMR signal.

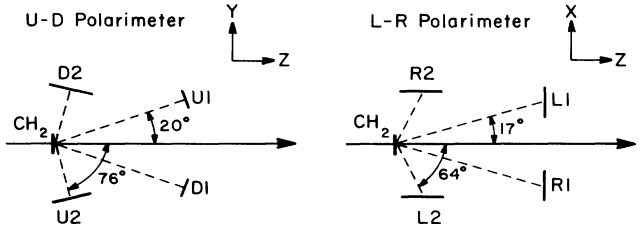

FIG. 2. Geometry for the up-down and left-right polarimeters. The drawing is not to scale.

The presence of the PTM field caused deflection of the incident proton beam by $148/p$ rad and a deflection of the reaction products by $160/p$ rad, where p is the particle momentum (MeV/c). Typical deflections were 5.8° (7.8°) for the beam at the center of the target, and 24°(42.7°) for the pions emerging at $\theta_\pi^* = 90°$ at beam energies of 800 (500) MeV. The deflection of the pions by the PTM limited the c.m. angles that could be measured to $\theta_\pi^* \leq 110°$.

C. Spectrometer

The elements of the spectrometer were a magnet (M) giving nominal horizontal deflection of 22°, four multiwire proportional chambers (W1–W4) for determination of the deuteron orbit through the magnet, and scintillators S1 and S2-S3 for measurement of the time of flight (TOF) of the deuteron. Since the deuterons are confined by kinematics to a cone of laboratory half-angle $\sim$15°, magnet M was a "C magnet" with its yoke on the large-angle side of the experiment. The minimum angle that the spectrometer could reach limited the c.m. angles that could be measured to $\theta_\pi^* \leq 150°$.

Each of the multiwire proportional chambers (MWPC's: W1–W4) contained two planes, with vertical and horizontal sense wires, respectively. The 2-mm sense-wire spacing gave x and y coordinates of the deuteron path at each chamber location. The overall momentum resolution of the spectrometer was observed to be $\sim$3%. Its angular acceptance in the laboratory was 9° horizontally and 6° vertically. The TOF measurement given by S1 and S2-S3 in conjunction with the momentum measurement provided easy mass discrimination between deuterons and other charged particles as shown in Fig. 3.

D. Recoil counter

The recoil counter used for detection of the pions consisted of two MWPC's (W5, W6) and a scintillator plane (S4–S7). The time resolution for each scintillator was improved by time averaging of photomultiplier tube signals from opposite ends. The MWPC's were of the same construction as the spectrometer MWPC's. The recoil counter had a laboratory angular acceptance of 24° horizontally and 18° vertically. It was located about 0.5 m from the center of the target, as a compromise between angular acceptance, TOF resolution, and avoidance of stray fields from the PTM. The TOF in the recoil arm was determined relative to the signal from S1. Consequently, it contained an admixture of the deuteron TOF. In spite of this effect, particle identification with the

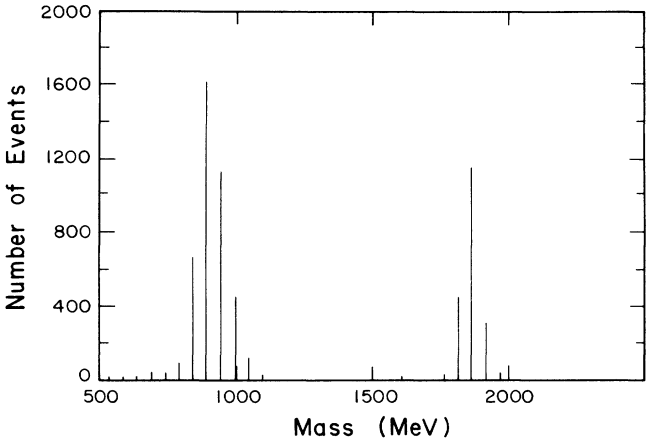

FIG. 3. Mass spectrum from the spectrometer.

recoil TOF was easily attained, since the fast pions were well separated from the slower protons and deuterons in the recoil arm.

E. Trigger logic

The trigger logic (somewhat simplified in the following discussion) was at two levels. First, a fast gate (FG) was formed that required coincident detection of charged particles in the scintillators of both the spectrometer and the recoil counter. A spectrometer gate (SG) signal was generated by requiring coincidence between S1 and the logical OR of S2 and S3. A recoil counter gate (RG) signal was generated by the logical OR of S4–S7 signals. The FG signal was generated by a coincidence between the SG and RG signals and was used to initiate conversion in analog-to-digital (ADC's) and time-to-digital converters (TDC's) that provided pulse height and TOF information for both particles. The relative timing of the gates was arranged so that all timing was done relative to the S1 signal. The presence of the FG signal also triggered an examination of the wire-chamber information. A signal (FGA) of rate proportional to the rate of accidental FG signals was generated by a second logic network similar to the above, but having the RG signal delayed by ~ 128 ns relative to the SG signal.

At the second level, fast discriminator output signals from each plane of the wire chamber system were sent to a logic network that required signals from three of the four spectrometer x planes and three of the four y planes, along with signals from both x and y planes of W5 or W6. When these conditions were met, a master gate (MG) signal was generated that inhibited further input to the electronics, sent a write gate to the wire chamber electronics, and signaled the computer to read the event. If the conditions were not met, a fast clear (FC) signal was generated to reject the event, clearing the TDC's and ADC's. Since this process required several microseconds, the inputs to the electronics were inhibited for a fixed 4 μs in order to provide a measure of the dead time due to rejected events. A signal (MGA) of rate proportional to the rate of accidental MG signals was generated by a duplicate logic network with the recoil signals delayed by 128 ns relative to the spectrometer signals.

F. Experimental procedure

At each beam energy, the steering magnets were used to position the beam on the target by the photographic exposure method outlined above. The position and shape of the aligned beam at the profile monitors were then noted and continuously monitored. The monitor polarimeter was then centered on the new beam position by minimizing the geometric asymmetry measured in the L-R polarimeter. At each spectrometer angle setting, the beam current was adjusted in order to maintain uninhibited (live) times greater than 60%. Because of the large asymmetries, it was important to monitor the live time for each spin orientation in order to avoid large systematic errors due to changes in the efficiency of the system for the different spin orientations. As stated earlier, beam currents of 0.5–1.5 pA were typical. Typical instantaneous rates for some of the above trigger signals were

$$\text{RG}\sim 1.6\ \text{MHz/pA},\quad \text{SG}\sim 0.2\ \text{MHz/pA},$$

$$\text{FG}\sim 8.0\ \text{kHz/pA},\quad \text{MG}\sim 5.0\ \text{kHz/pA},$$

$$\text{FC}\sim 3.0\ \text{kHz/pA},\quad \text{FGA}\sim 7.0\ \text{kHz/pA},$$

$$\text{MGA}\sim 3.0\ \text{kHz/pA}.$$

A large part of the contribution to the accidental rates came from the large background of pp elastic scattering.

The orientation of the beam polarization was reversed every minute automatically at the ion source. This orientation was tagged for each event written onto tape. During each spin reversal, the beam current was "quenched" for approximately 10 s, in order to provide a quench-ratio measurement of the magnitude of the beam polarization (see Sec. III C). Since reversing the target polarization required about 30 min, the target polarization was reversed only once every two data runs, which corresponded to once every few hours. Some of the 500- and 800-MeV data were taken with target reversals once every 4 or 5 h, and these data show greater sensitivity to systematic errors from the target polarization. The target polarization was measured once every 3 min during the data runs and recorded separately on magnetic tape. Because of the small beam current, there was never a problem of depolarization resulting from excessive heating or radiation damage in the target.

Carbon background measurements were made for $\theta_\pi^* = 38°$ and at the 500- and 800-MeV beam energies. These were done by removing the target beads physically and replacing them with hollow graphite beads of approximately the same density as the target beads. These runs were not used to subtract the quasifree events, but rather to verify that the fitting procedure for removal of the background was valid (see Sec. III B).

III. DATA ANALYSIS

The data analysis was accomplished in four major steps. First, the $pp \rightarrow d\pi^+$ data were separated from the

large background of pp elastic scattering events. Events were considered "perfect" if each MWPC plane had one and only one contiguous group of hits. "Deficient" events had to be corrected. These "deficient" events occurred when one or more wire planes registered either no hit (activated sense wire) or more than one group of hits. The event trigger was designed to accept some of these when enough information was present to analyze the data without good information from all planes. The requirements of two-body kinematics for the $pp \rightarrow d\pi^+$ reaction were used to remove most background, except that from quasifree events (p "p" $\rightarrow d\pi^+$, where "p" is a proton bound in a nucleus). Second, this quasifree background was subtracted from the signal histograms by a fitting procedure (see Secs. III A and III B). Third, the beam polarization was determined by calibrating the beam monitor with a quench-ratio measurement (see Sec. III C). Finally, the target polarization was determined from the NMR data and cross-checked against the beam polarization using the assumed relation between A_{no} and A_{on} (see Sec. III D). The known analyzing power for elastic pp scattering was also used to verify the NMR measurement of the target polarization.

A. Correction of deficient MWPC data

The corrections for deficient MWPC data were made separately for the spectrometer and the recoil counter. For the spectrometer, a deficient x value (anything but a single hit in each of the x planes) meant that either the entrance or exit trajectory was indeterminate. With three good x values it is possible to track the particle through the known magnetic field,[41] but the tracking approach was replaced by one that took considerably less computer time. The spectrometer magnetic field was of sufficient uniformity to have a fairly well-defined symmetry plane. This plane is defined as the locus of points at which the asymptotic entrance and exit trajectories of the individual particles intersect (or most nearly intersect). These points will fall onto a two-dimensional plane of insignificant thickness if the magnetic field is uniform. The position and "thickness" (deviation from two dimensionality) of this plane was measured using the "perfect" wire-chamber data. The plane was found to be only ~ 1 mm in thickness and to coincide with the midplane of the magnet. An approximate value for a missing x coordinate could be calculated easily by finding the intersection of the asymptotic trajectory defined by two of the good x coordinates and the symmetry plane and using that point and the third good x coordinate to determine the other trajectory. When the event was deficient because of multiple hits rather than a missing hit in a single x plane, the hit value closest to the calculated value was used for the final trajectory information. Deficient data from a single y plane could be corrected directly because no significant vertical deflection of the trajectories was observed.

A missing coordinate from one of the recoil counter chambers was provided by the strong correlation between the hit positions observed in the two recoil chambers. The uncertainty in the correlation between the two x- or y-plane hits is primarily due to multiple scattering in the target cryostat and is magnified by the deflection of the pions by the PTM field. Again, "perfect" data were used to measure the correlation functions for the x and y planes at each energy and angle setting. Once the correlation functions were known, the missing data could be calculated directly; the values were randomized within a range of $\pm\sigma$ about the correlation function in order to reproduce the uncertainty of the actual data.

These corrections were checked by taking perfect events and randomly eliminating one of the coordinates to simulate deficient events. These deficient coordinates were then "corrected" according to the above method and analyzed by normal procedures, the resulting "signal" histogram being compared with the signal histogram produced by normal analysis of the original perfect data. A typical result is shown in Fig. 4. By including these deficient events in the data, the number of analyzable events was increased by 40% and, to first order, any false asymmetry resulting from rejected events due to bad wire planes was removed.

Initial selection of $pp \rightarrow d\pi^+$ events from the large background of protons from pp elastic scattering was accomplished when only those events with a pion in the recoil counter were kept. The recoil counter TOF was used to make this selection, which included a small class of three body final state events, $pp \rightarrow pn\pi^+$, $pp \rightarrow d\pi^0\pi^+$, and $pp \rightarrow pp\pi^0$, as well as some accidental coincidences.

The kinematic constraints of the reaction were overdetermined, since the laboratory angles θ,ϕ of both particles as well as the momentum of the deuteron were measured. These parameters, along with the known beam energy and conservation of energy and momentum, provide more than enough data to fix the six degrees of freedom. As a result the unique selection of the $pp \rightarrow d\pi^+$ final state was made from all other competing reactions except for the quasifree scattering, p "p" $\rightarrow d\pi^+$, where "p" represents a proton bound in a complex nucleus.

Histograms of certain quantities were used as signal histograms, because they exhibited a relatively sharp

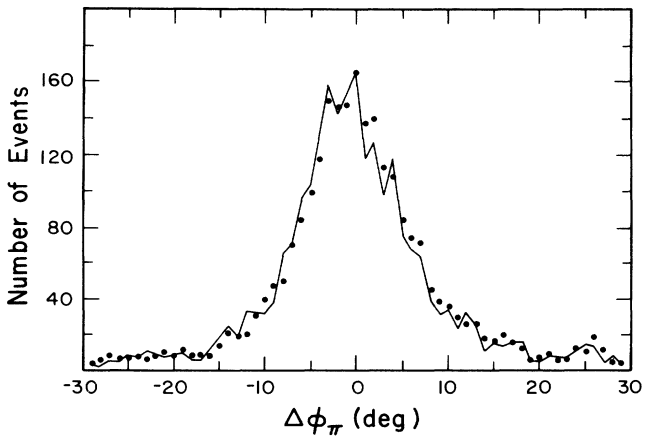

FIG. 4. Comparison of perfect MWPC events (curve) with their deficient counterparts (points).

peak due to the $pp \rightarrow d\pi^+$ events superimposed on a broad background due to other reactions, primarily the quasifree p "p" $\rightarrow d\pi^+$ events. These histograms were for the differences

$$\Delta\theta_d = \theta_d(\text{measured}) - \theta_d(\text{predicted}) ,$$

$$\Delta\theta_\pi = \theta_\pi(\text{measured}) - \theta_\pi(\text{predicted}) ,$$

and

$$\Delta\phi_\pi = \phi_\pi(\text{measured}) - \phi_\pi(\text{predicted}) .$$

The predictions for θ_π and ϕ_π were obtained from the deuteron trajectory in conjunction with the $pp \rightarrow d\pi^+$ kinematics. The prediction for θ_d was similarly obtained from the pion trajectory. Other variables that were put into histograms were as follows: mass, momentum, missing mass, θ, and θ^* for the particle detected in the spectrometer; for the particle detected in the recoil counter, θ, θ^*, the TOF, and the pulse height. Furthermore, histograms were also made of recoil and spectrometer target projections, obtained by projection of the recoil or spectrometer trajectories through the field of the PTM to the plane of the target.

Event selection was made when selected cuts were put on variables appearing in the histograms of mass, missing mass, recoil target projection, and $\Delta\theta_\pi$ determined from the spectrometer data. This analysis yielded signal histograms $\Delta\phi_\pi$ of the type shown in Fig. 5. These histograms were sorted according to beam and target spin orientations and pion c.m. angle.

B. Quasifree background subtraction

The quasifree background appeared as a low broad distribution under the $pp \rightarrow d\pi^+$ peak in the $\Delta\phi_\pi$ histogram (Fig. 5). It was removed by a nonlinear least squares fit to the $\Delta\phi_\pi$ histograms with a Gaussian peak (representing the $pp \rightarrow d\pi^+$ events) and a quadratic polynomial (representing the quasifree background). In order to improve the statistical accuracy of the fit, all the data for a given spectrometer angle setting were summed into one histogram. The assumption was made that the background did not change rapidly with angle. The background was determined separately for each of the four beam-target spin combinations, since it could not be assumed that the background was independent of either spin.

The resulting fits for data at $\theta_\pi^* = 90°$ and 38° were compared with the $\Delta\phi_\pi$ histograms obtained in the background runs with a carbon target at 500 and 800 MeV. The 800-MeV results are shown in Fig. 6. It is seen that the background was indeed smoothly varying and well approximated by a quadratic polynomial. The background measurements also indicated that the fitting procedure gave an overestimate of the background by 20–30 %. This discrepancy was due to the modest ϕ resolution of the system (exhibited in Fig. 5), which made it difficult to separate the tails of the Gaussian peak from the background distribution. The fact that the background was overestimated by the fitting procedure was evidence that some signal had been included in the background. This inclusion had no effect on the final asymmetry as long as the fraction of the signal included in the background was the same for each spin orientation.

A check for the equality of these fractions was made by an independent background determination, based on the assumption that the target components contributing to this quasifree background were unpolarized. ^{13}C and ^3He possibly could have been polarized since the NMR signal was looked at only for ^1H. However, it is reasonable to assume that the ^3He was polarized to no greater than 1%, and that the ^{13}C, having a natural abundance of only 1.11%, would contribute negligibly. In this method, asymmetries of the background yields were calculated and used (along with the first order estimate of the signal asymmetry) to determine the amount of signal contained in the background. The estimated backgrounds then were revised and used to recalculate the signal asymmetries, which were compared with those originally obtained. Any significant difference between these asymmetries would indicate an error in the back-

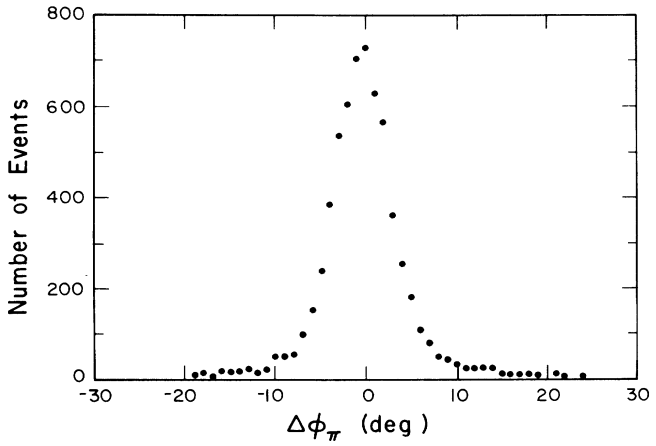

FIG. 5. Typical final $\Delta\phi_\pi$ spectrum for $\theta_\pi^* = 56°$ after analysis, but with background unsubtracted.

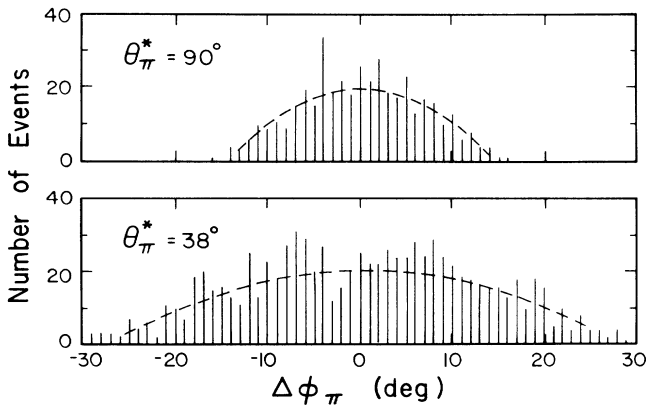

FIG. 6. Carbon background spectra showing quasifree background shape for $\theta_\pi^* = 90°$ and 38° with quadratic polynomial fit.

ground subtraction. All of the data were subjected to this test during the final analysis, and no significant discrepancy was found.

C. Monitor polarimeter calibration

The polarimeter used to monitor the beam polarization required calibration. Because of the properties of the Lamb-shift polarized ion source at LAMPF, a measure of the magnitude of the beam polarization could be obtained by measuring the "quench ratio,"[42] the ratio of "quenched" beam current to normal beam current. The "quenched" beam current is generated by turning off or "quenching" that part of the beam which has 100% polarization coming from the Lamb-shift source. Ideally, this quenched beam represents that fraction of the normal beam current which is unpolarized. The remaining beam current is assumed to be 100% polarized and oriented along a spatial direction determined by a "spin filter." In reality, the quenched beam has a small polarization (~ -0.03), and this must be taken into account in the final calculation of the beam polarization. Depolarization effects by the accelerator beam transport are known to be small.[42] The accelerator, however, does introduce "noise" into the system, in the form of beam current fluctuations that cause the "quench" value of the beam polarization to vary from run to run, even if the beam polarization remains constant. Since these effects are random, averaging over many runs largely eliminates this problem. For this experiment, only the left-right polarimeter was calibrated, the up-down polarimeter merely providing a monitor to verify that the polarization did not rotate from the vertical direction. The calibration was done at each of the six energies and compared with the calibration of a LAMPF facility polarimeter located upstream in the beam to verify that there were no systematic errors. The calibrated polarimeter was used to measure the beam polarization for each state of beam polarization for each run.

D. Target polarization

The NMR system used to monitor the target polarization was calibrated by making measurements of the thermal equilibrium (TE) polarization of the target at 1 K. This polarization can be calculated since it is the result of a Boltzmann distribution of the spin state populations. It is only $\sim 0.25\%$ and therefore the NMR signal is quite small. In order to obtain a statistically accurate result, 256 successive frequency sweeps across the NMR signal peak were accumulated in a frequency spectrum. A subtraction was needed to remove the curvature of the background. This subtraction was achieved by altering the magnetic field in order to move the signal peak outside the frequency range swept and subtracting 256 background sweeps from the original spectrum. Twenty such measurements were made for a given calibration, and calibration measurements were made weekly throughout the whole data taking period.

From the known target polarization and the measured NMR signal area, a calibration constant could be calculated. Because of the smallness of the TE signal, the amplifier requires a large gain change ($\times 5120$) between the TE calibrations and the enhanced polarization measurements, and it was easy for a systematic error in the procedure to make the overall normalization of the target polarization uncertain.

This normalization was checked by two methods as follows: (1) The asymmetry in pp elastic scattering could be used to measure the target polarization since the pp analyzing power is well known; and (2) the symmetry relation $A_{no}(\theta) = -A_{on}(\pi - \theta)$ makes possible a measurement of the target polarization in terms of the known beam polarization. Both procedures were used and both confirmed discrepancies of $\sim 6\%$ in the 650-MeV data and in some of the 500- and 800-MeV data. The cause of these discrepancies is not known, but they may be due to physical changes in the target cell resulting from improper cryogenic changeover of the target from the TE to the enhanced polarization condition. The pp analyzing-power data indicate that these discrepancies occurred suddenly and remained constant over the span of several TE measurements. The precision of the NMR measurements was determined by the standard deviation of the mean of the TE measurements, which was consistently of the order of 2%.

E. Systematic errors

The uncertainty of the overall normalization of the data was determined by the uncertainty in knowledge of the absolute values of the beam and target polarizations. For the beam polarization, this was limited by the accuracy of the quench-ratio calibration, which usually was good within 2%. The accuracy of the target polarization was limited by the uncertainty in knowledge of the analyzing power for pp elastic scattering at these energies ($< 5\%$), since pp elastic scattering was used to normalize the target polarization for some of the data. Therefore, there are systematic errors of 2% in the A_{no} data, 5% in the A_{on} data, and 5.5% (beam and target errors added in quadrature) in the A_{nn} data.

IV. RESULTS AND DISCUSSION

The data are given numerically in Table I and graphically in Figs. 7–10. The actual energy values that are represented by 500, 600, 650, 700, 733, and 800 MeV, that take into account energy losses (~ 4 MeV), are 492, 593, 643, 695, 729, and 796 MeV, respectively, with an uncertainty of ± 2 MeV. The spectrometer angle settings were known to within $\pm 1°$. In the analyzing-power data (Figs. 7 and 8), the symmetry relationship $A_{no}(\theta_\pi^*) = -A_{on}(\pi - \theta_\pi^*)$ is used to show the A_{no} data (solid circles) and the A_{on} data (open circles) on one plot of A_n ($= A_{no}$) for each energy. Similarly, in the spin-correlation data (Figs. 9 and 10), use is made of the symmetry relationship $A_{nn}(\theta_\pi^*) = A_{nn}(\pi - \theta_\pi^*)$ to show the forward angle A_{nn} data (solid circles) and the backward angle data (open circles) on a single plot for each energy. The analyzing-power data agree well with those of Saha *et al.*[37] throughout the energy region, and the spin correlation data agree well with the only other A_{nn} data available, those of Aprile *et al.*[35] near 500 MeV, also

TABLE I. Experimental results for A_{no}, A_{on}, and A_{nn}.

θ_π^*	A_{no}	A_{on}	A_{nn}
		500 MeV	
36.5±0.9	0.220±0.013	−0.171±0.014	−0.876±0.015
44.5±0.7	0.243±0.014	−0.158±0.013	−0.855±0.014
47.9±0.9	0.223±0.020	−0.126±0.017	−0.866±0.018
51.6±0.7	0.223±0.014	−0.140±0.014	−0.844±0.015
55.4±0.7	0.177±0.019	−0.128±0.016	−0.902±0.016
63.0±0.8	0.148±0.017	−0.093±0.016	−0.910±0.016
72.8±0.7	0.107±0.028	−0.042±0.026	−0.915±0.030
79.1±0.5	0.035±0.029	0.015±0.026	−0.931±0.029
84.9±0.5	−0.001±0.029	0.023±0.026	−0.937±0.029
84.9±0.7	−0.079±0.028	0.054±0.029	−0.945±0.028
87.5±0.4	−0.033±0.040	0.068±0.040	−0.935±0.043
93.0±0.4	−0.060±0.042	0.066±0.040	−0.900±0.045
96.6±0.7	−0.074±0.028	0.011±0.030	−0.925±0.030
97.3±1.0	−0.029±0.040	0.025±0.040	−0.932±0.043
107.5±1.0	0.027±0.028	−0.106±0.029	−0.910±0.030
		600 MeV	
30.5±1.1	0.399±0.008	−0.288±0.019	−0.866±0.010
37.3±0.8	0.450±0.008	−0.338±0.014	−0.853±0.010
43.9±0.8	0.483±0.008	−0.371±0.019	−0.851±0.010
44.1±1.7	0.480±0.015	−0.372±0.034	−0.855±0.018
52.6±1.3	0.488±0.015	−0.363±0.034	−0.848±0.018
60.5±1.3	0.479±0.015	−0.384±0.034	−0.858±0.018
67.7±1.3	0.457±0.020	−0.398±0.025	−0.873±0.020
74.4±1.1	0.392±0.020	−0.366±0.025	−0.906±0.020
81.2±1.2	0.394±0.020	−0.386±0.025	−0.958±0.020
81.3±0.8	0.380±0.020	−0.341±0.025	−0.966±0.020
87.5±0.5	0.398±0.020	−0.378±0.025	−0.986±0.020
92.9±0.5	0.362±0.020	−0.342±0.025	−0.981±0.020
99.7±1.2	0.353±0.020	−0.396±0.025	−1.004±0.020
105.0±0.8	0.395±0.020	−0.422±0.025	−0.965±0.020
109.0±0.7	0.371±0.020	−0.398±0.025	−0.974±0.020
		650 MeV	
31.9±0.7	0.463±0.008	−0.290±0.008	−0.855±0.009
40.0±0.6	0.505±0.008	−0.334±0.008	−0.832±0.009
45.2±1.6	0.482±0.023	−0.346±0.025	−0.825±0.029
47.8±0.5	0.519±0.008	−0.367±0.008	−0.824±0.009
53.6±1.3	0.492±0.022	−0.376±0.025	−0.856±0.027
61.8±1.4	0.454±0.023	−0.385±0.025	−0.859±0.027
64.7±1.3	0.457±0.049	−0.392±0.049	−0.855±0.062
71.7±1.2	0.446±0.049	−0.407±0.048	−0.907±0.058
78.8±1.3	0.460±0.048	−0.420±0.047	−0.956±0.055
82.3±0.6	0.464±0.022	−0.469±0.022	−1.017±0.026
88.7±0.5	0.436±0.022	−0.428±0.022	−1.036±0.025
94.2±0.4	0.467±0.022	−0.431±0.022	−1.011±0.026
		700 MeV	
32.4±1.5	0.376±0.018	−0.216±0.020	−0.811±0.023
40.2±1.3	0.410±0.017	−0.277±0.020	−0.796±0.023
45.4±1.0	0.404±0.014	−0.291±0.016	−0.782±0.019
47.8±1.2	0.419±0.018	−0.309±0.020	−0.783±0.023
53.7±0.9	0.384±0.014	−0.310±0.016	−0.796±0.019
61.6±0.9	0.370±0.014	−0.351±0.016	−0.831±0.018
69.1±1.3	0.368±0.010	−0.386±0.015	−0.850±0.010
75.9±1.1	0.369±0.010	−0.406±0.015	−0.912±0.010
82.2±0.5	0.369±0.016	−0.410±0.018	−0.926±0.020
82.4±1.1	0.363±0.010	−0.404±0.015	−0.981±0.010
88.5±0.3	0.409±0.018	−0.399±0.019	−1.006±0.020
94.0±0.3	0.392±0.017	−0.362±0.019	−0.995±0.020
96.7±1.2	0.416±0.060	−0.368±0.076	−0.957±0.104
100.4±0.6	0.384±0.042	−0.368±0.047	−0.945±0.049

TABLE I. (*Continued.*)

θ_π^*	A_{no}	A_{on}	A_{nn}
102.5±0.9	0.458±0.058	−0.388±0.078	−0.952±0.107
105.9±0.5	0.413±0.042	−0.380±0.047	−0.910±0.052
107.3±0.7	0.395±0.064	−0.377±0.079	−0.882±0.112
110.0±0.4	0.417±0.042	−0.373±0.048	−0.886±0.054
		733 MeV	
31.8±0.6	0.327±0.014	−0.196±0.015	−0.776±0.016
39.5±0.5	0.362±0.013	−0.227±0.014	−0.776±0.015
44.7±0.9	0.373±0.012	−0.302±0.013	−0.763±0.016
47.4±0.5	0.370±0.013	−0.255±0.014	−0.745±0.016
52.9±0.9	0.366±0.012	−0.330±0.012	−0.758±0.015
61.7±0.9	0.334±0.012	−0.352±0.012	−0.802±0.015
67.8±0.7	0.286±0.027	−0.350±0.029	−0.820±0.029
74.9±0.7	0.322±0.025	−0.380±0.028	−0.876±0.030
82.0±0.9	0.300±0.046	−0.384±0.042	−0.939±0.061
82.2±0.7	0.312±0.026	−0.361±0.028	−0.917±0.030
88.7±0.7	0.324±0.042	−0.332±0.043	−1.008±0.053
94.3±0.6	0.343±0.041	−0.309±0.044	−1.013±0.052
100.1±0.6	0.350±0.024	−0.321±0.028	−0.945±0.030
105.8±0.4	0.357±0.024	−0.291±0.028	−0.915±0.032
110.1±0.3	0.371±0.024	−0.309±0.029	−0.880±0.033
		800 MeV	
30.2±0.6	0.261±0.009	−0.127±0.022	−0.785±0.024
38.0±0.5	0.284±0.021	−0.200±0.020	−0.759±0.022
43.8±0.8	0.254±0.010	−0.221±0.011	−0.737±0.012
46.2±0.5	0.276±0.008	−0.194±0.020	−0.726±0.022
52.7±0.7	0.254±0.011	−0.246±0.011	−0.744±0.012
59.4±0.5	0.234±0.011	−0.265±0.010	−0.760±0.011
61.6±0.7	0.223±0.011	−0.270±0.011	−0.750±0.012
67.1±0.5	0.194±0.010	−0.265±0.010	−0.816±0.011
71.2±0.6	0.222±0.017	−0.330±0.026	−0.841±0.030
75.4±0.6	0.198±0.010	−0.289±0.010	−0.894±0.010
78.2±0.5	0.231±0.016	−0.314±0.025	−0.903±0.029
82.2±0.4	0.220±0.015	−0.283±0.028	−0.887±0.018
85.3±0.5	0.254±0.016	−0.308±0.025	−0.954±0.028
88.3±0.4	0.243±0.015	−0.254±0.028	−0.954±0.016
94.2±0.5	0.260±0.014	−0.240±0.014	−0.933±0.016
94.5±0.4	0.304±0.013	−0.249±0.026	−0.964±0.015
100.5±0.3	0.291±0.014	−0.181±0.014	−0.920±0.016
105.4±0.3	0.300±0.014	−0.178±0.014	−0.871±0.017

shown in Fig. 9 as solid and open square data points.

Also shown in Figs. 7 and 9 are the predictions or fits given by the partial-wave analyses (PWA's) of Bugg[43] (labeled B in the figures) and the Osaka group[44,45] (labeled H and $\mathrm{HWY}_{D(S)}$). The subscripts D and S refer to their two solutions. The B and H solutions in Fig. 7 also bracket the Saha *et al.* data very well and therefore serve to compare the present data to Saha *et al.* The dotted curves show two 800-MeV A_{nn} predictions of the Osaka group,[44] made before the data of this experiment and the companion A_{ll} and A_{sl} experiment[38] became available; the solid curves show the fits obtained when these data were included in the PWA's. The partial-wave solutions have been clearly influenced by these data, as indicated by the contrast between the dotted and solid curves. As would be expected for such phenomenological analyses, the solid-line fits are relatively good for both A_n and A_{nn}. Exception might be taken in the 733-MeV A_n data near 120°. The three points off the PWA curves were taken in a single spectrometer angle setting. However, if the systematic error (5%) is taken into account, these data are within two standard deviations of the trend given by the PWA's. It should be noted that Bugg permits a renormalization of the data at each energy, consistent with an uncertainty in the target polarization. These renormalization factors range between 3% and 10%. Bugg finds the partial-wave amplitudes to be interpretable very simply without invoking dibaryons, in terms of $\pi d \rightarrow N\Delta$, with the nucleon being simply a spectator. By contrast, the Osaka group finds that a three-channel (pp, $N\Delta$, πd) K-matrix analytic continuation of the scattering amplitude in the complex en-

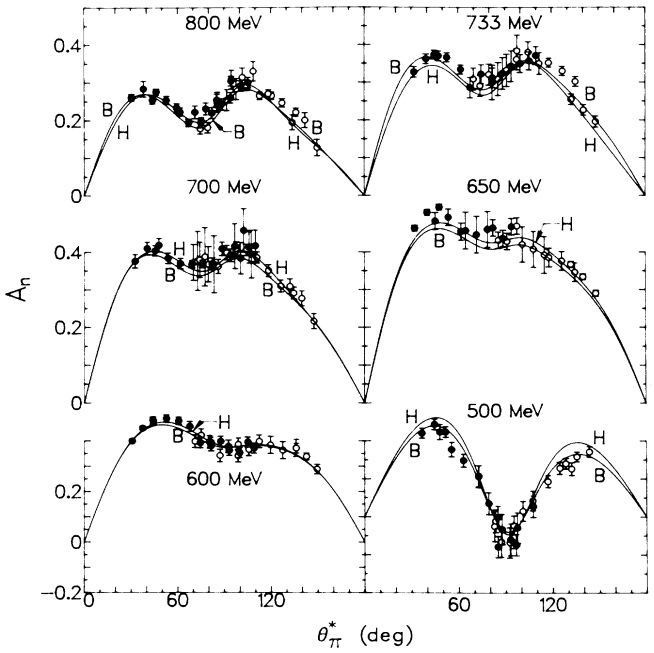

FIG. 7. Analyzing-power data compared to PWA's. Solid circles are the A_{no} data, open circles are the A_{on} data. Curves are the latest PWA's by Bugg (B) and the Osaka group (H).

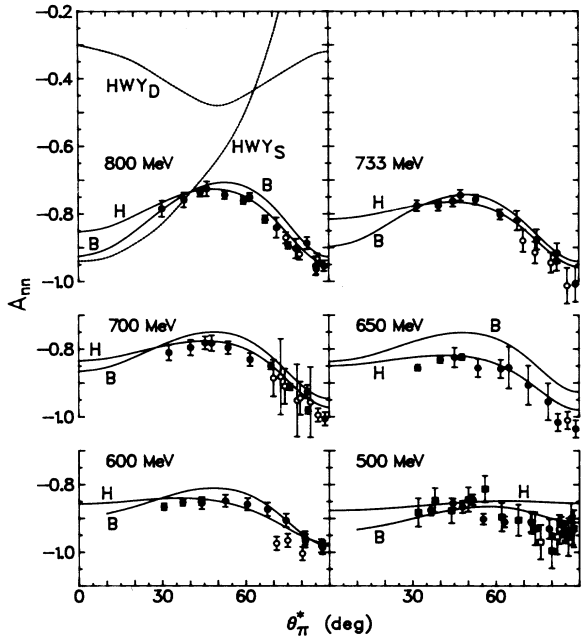

FIG. 9. Spin correlation data compared to PWA's. Circles are the present data and the squares are from Aprile *et al.* (Ref. 35). H and B are the same as defined in Fig. 7. The two dotted curves ($HWY_{D(S)}$) refer to solutions of the Osaka group before these data were available.

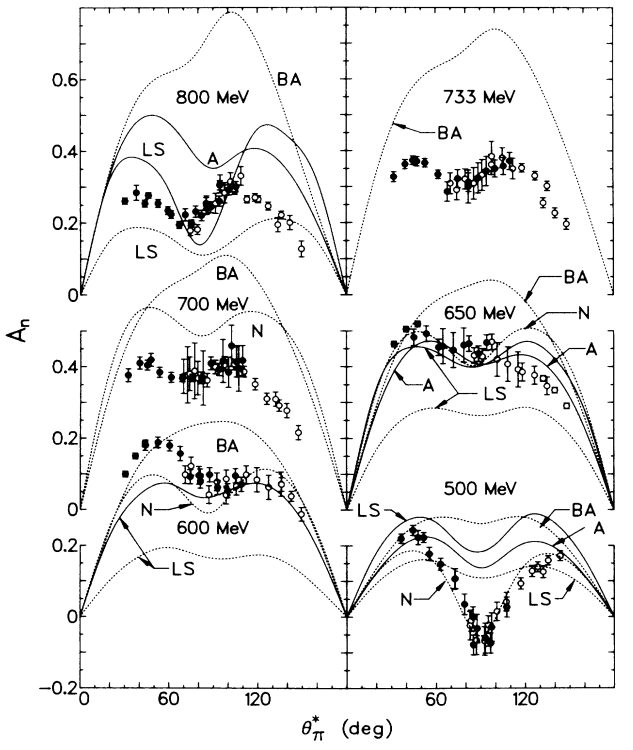

FIG. 8. Analyzing-power data compared to model calculations. See text for the definitions of the symbols. The dotted curves are calculations without this data, solid curves are calculations done with consideration of the present data.

ergy plane using their PWA leads to poles in the NN mass regions 2170 and 2250 MeV.[45]

The curves shown in Figs. 8 and 10 are the predictions of various model calculations. The dotted curves show predictions made before the present data (and those of Ref. 38) became available; the dashed curves show pre-

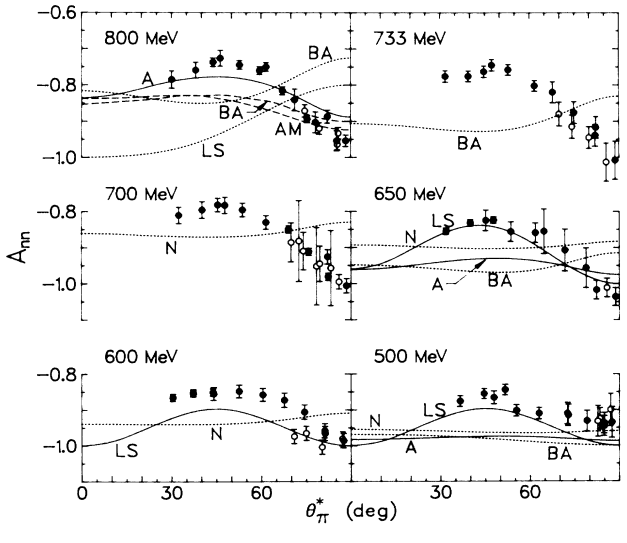

FIG. 10. Spin correlation data compared to model calculations. See text for the definitions of the symbols. Solid and dotted curves are the same as in Fig. 8. The dashed curves (AM and BA) were done with consideration of preliminary data from this experiment.

dictions influenced by preliminary data from these experiments, and the solid curves show predictions based on the final data values. The predictions of Blankleider and Afnan,[9,46] labeled BA, are the results of coupled-channel calculations that maintain two- and three-body unitarity but are nonrelativistic. The curves labeled AM are predictions of Ref. 20, and those labeled A are new predictions from Afnan[47] that use the P_{11} potential M1 of Afnan and McLeod[20] and include "all S-, P-, and D-wave N-N interactions, and S- and P-wave π-N interactions in the πNN part of the Hilbert space." The curves labeled N are the results of a coupled-channel calculation by Niskanen,[5] also nonrelativistic, which gives predictions up to 720 MeV. The curves labeled LS are the results of a relativistic perturbation calculation by Locher and Švarc,[12] which does not preserve three-body unitarity.

The A_n predictions of Niskanen[5] (curves N of Fig. 8) were made before the present data were available. They have the correct sign and magnitude, but do not exhibit the forward-backward asymmetry seen in the data. The initial A_n predictions of Blankleider and Afnan[9] (dotted curves BA of Fig. 8) are asymmetric, but in the wrong direction, and are consistently too large. The most recent predictions of that group (solid curves A of Fig. 8) fit the data reasonably well at 650 MeV and have qualitatively the right shape at 800 MeV, but not at 500 MeV. The A_n predictions of Locher and Švarc using their standard model (dotted curves LS of Fig. 8) have only qualitative similarity to the data, but results that they obtained by *ad hoc* modifications of the small p-p spin triplet amplitudes, T_2 and T_3, and adjustment of the pion range parameter (solid curves LS) give a much better fit, except at 500 and 800 MeV. However, the significance of these modifications is not understood and does not imply or even suggest the need for dibaryons.

V. CONCLUSIONS

The results presented here are the first measurements of A_{nn} for the reaction $pp \rightarrow d\pi^+$ in the energy range 500–800 MeV. These data make a significant contribution to the determination of better partial-wave solutions, but are unable to discriminate between the two partial-wave treatments presently employed.

From our previously reported 90° results[25] it appeared that the theory of Blankleider and Afnan[9] underestimated the triplet contribution (T_6 in Fig. 3 of Ref. 25). This deficiency seems to be substantiated by the PWA's,[43–45] and can be discerned by the apparent presence of higher order cosine terms in the angular distributions of the data as compared with those present in various theoretical predictions.

The fact that the excitation function of T_2 (Fig. 3 of Ref. 25) lacks any significant structure indicates that the resonancelike behavior in T_6, suspected to be caused by the $^3F_3$ dibaryon, is more likely caused by threshold effects.[24] Since T_2 should show effects due to a $^3F_3$ while T_6 should not,[24] more measurements of A_{nn} and A_{ll} need to be made between 700 and 800 MeV in smaller energy steps. Furthermore, in order for PWA's to become sufficiently reliable to determine the small triplet amplitudes at all angles, still more data are needed, especially in the 700- to 800-MeV region. These amplitudes are difficult to determine because of the dominance of the Δ resonance, which is driven by the $^1D_2$ partial wave.

In conclusion, although sufficient data are not available to establish the partial-wave amplitudes firmly over the entire energy region from 500 to 800 MeV, the data presented here point to the inadequacies of the current theories. Since these theories do not incorporate relativistic effects completely, however, and are not in agreement about how to treat the P_{11} π-N pole term, the inclusion of $^1D_2$ or $^3F_3$ resonances would appear to be premature.

ACKNOWLEDGMENTS

We are thankful for the considerable attention given to the needs of this experiment by the LAMPF operations, cryogenic, and secondary beamline support groups. We also express our appreciation to the computer staff at LAMPF. This work was supported, in part, by the U.S. Department of Energy.

---

*Present address: University of Virginia, Charlottesville, VA 22901.

†Present address: Los Alamos National Laboratory, Los Alamos, NM 87545.

‡Present address: Texas A&M University, College Station, TX 77843.

§Present address: George Washington University, Washington, D.C. 20052.

[1]M. Gell-Mann and K. Watson, Annu. Rev. Nucl. Sci. **4**, 219 (1954).

[2]A. H. Rosefeld, Phys. Rev. **96**, 130 (1954).

[3]F. Mandl and T. Regge, Phys. Rev. **99**, 1478 (1955).

[4]S. Mandelstam, Proc. R. Soc. London, Ser. A **244**, 491 (1958).

[5]J. A. Niskanen, Nucl. Phys. **A298**, 417 (1978); Phys. Lett. **71B**, 40(1977); **79B**, 190 (1978); **82B**, 187 (1979); **141B**, 301 (1984).

[6]T. Mizutani and D. S. Koltun, Ann. Phys. (N.Y.) **109**, 1 (1977).

[7]A. S. Rinat, Nucl. Phys. **A287**, 399 (1977).

[8]Y. Avishai and T. Mizutani, Nucl. Phys. A **352**, 399 (1981); **A326**, 352 (1979); **A338**, 377 (1980).

[9]I. R. Afnan and B. Blankleider, Phys. Lett. **93B**, 367 (1980); B. Blankleider and I. R. Afnan, Phys. Rev. C **24**, 1572 (1981).

[10]A. S. Rinat, Y. Starkand, E. Hammel, and A. W. Thomas, Phys. Lett. **80B**, 166 (1979); A. S. Rinat, Y. Starkand, and E. Hammel, Nucl. Phys. **A364**, 486 (1981).

[11]C. Fayard, G. H. Lamot, and T. Mizutani, Phys. Rev. Lett. **45**, 524 (1980); T. Mizutani, C. Fayard, G. H. Lamot, and R. S. Nahabetian, Phys. Lett. **107B**, 177 (1981); G. H. Lamot, J. L. Perrot, C. Fayard, and T. Mizutani, Phys. Rev. C **35**, 239 (1987); T. Mizutani, B. Saghai, C. Fayard, and G. H. Lamot, *ibid.*, **35**, 667 (1987).

[12]M. P. Locher and A. Švarc, J. Phys. G **11**, 183 (1985); W.

Grein, A. König, P. Kroll, M. P. Locher, and A. Švarc, Ann. Phys. (N.Y.) **153**, 301 (1984).
[13]P. J. Mulders, Phys. Rev. D **25**, 1269 (1982).
[14]W. Grein, K. Kubodera, and M. P. Locher, Nucl. Phys. **A356**, 269 (1981).
[15]A. Yokosawa, Phys. Rep. **64**, 47 (1980); J. Bystricky *et al.*, Phys. Lett. **142B**, 130 (1984); F. Perrot *et al.*, Nucl. Phys. **B278**, 881 (1986).
[16]J. Bolger *et al.*, Phys. Rev. Lett. **46**, 167 (1981).
[17]K. Kubodera, M. P. Locher, F. Myhrer, and A. W. Thomas, J. Phys. G **6**, 171 (1980).
[18]R. Bhandari, R. A. Arndt, L. D. Roper, and B. J. VerWest, Phys. Rev. Lett. **46**, 1111 (1981).
[19]B. J. Edwards and G. H. Thomas, Phys. Rev. D **22**, 2772 (1980).
[20]I. R. Afnan and R. J. McLeod, Phys. Rev. C **31**, 1821 (1985).
[21]J. H. Gruben and B. J. VerWest, Phys. Rev. C **28**, 836 (1983).
[22]R. Vinh Mau, Nucl. Phys. **A374**, 3c (1982).
[23]C. L. Hollas, Phys. Rev. Lett. **44**, 1186 (1980).
[24]F. Foroughi, J. Phys. G **8**, 1345 (1982); **10**, 617 (1984).
[25]G. Glass *et al.*, Phys. Rev. Lett. **53**, 1984 (1984).
[26]C. Richard-Serre *et al.*, Nucl. Phys. **B20**, 413 (1970).
[27]M. G. Albrow *et al.*, Phys. Lett. **34B**, 337 (1971).
[28]H. Nann *et al.*, Phys. Lett. **88B**, 257 (1979).
[29]J. Hoftiezer *et al.*, Phys. Lett. **100B**, 462 (1981); Nucl. Phys. **A412**, 286 (1984).
[30]P. Walden *et al.*, Phys. Lett. **81B**, 156 (1979).
[31]E. Aprile *et al.*, Nucl. Phys. **A335**, 245 (1980).
[32]B. Mayer *et al.*, Nucl. Phys. A **437**, 630 (1985).
[33]J. Boswell *et al.*, Phys. Rev. C **25**, 2540 (1982).
[34]E. Aprile *et al.*, Nucl. Phys. A **379**, 369 (1982).
[35]E. Aprile *et al.*, Nucl. Phys. **A415**, 365 (1984).
[36]J. Hoftiezer *et al.*, Nucl. Phys. **A412**, 273 (1984).
[37]A. Saha *et al.*, Phys. Rev. Lett. **51**, 759 (1983).
[38]G. Glass *et al.*, Phys. Rev. C **31**, 288 (1985); D. Barlow *et al.*, (unpublished).
[39]A. B. Laptev and I. I. Strakovsky, A Collection of Experimental Data for the $pp \rightleftarrows d\pi^+$ Process, Academy of Sciences of the USSR, Leningrad Nuclear Physics Institute, Leningrad, 1985 (unpublished).
[40]J. Boissevain and W. B. Tippens, Los Alamos National Laboratory Report LA-9429-MS, 1983 (unpublished).
[41]M. L. Evans *et al.*, Phys. Rev. C **26**, 2525 (1982).
[42]M. McNaughton *et al.*, Phys. Rev. C **23**, 1128 (1981).
[43]D. Bugg, J. Phys. G **10**, 47 (1984); **10**, 717 (1984), and private communication.
[44]N. Hiroshige, W. Watari, and M. Yonezawa, Prog. Theor. Phys. **68**, 2074 (1982).
[45]N. Hiroshige, W. Watari, and M. Yonezawa, Prog. Theor. Phys. **72**, 1146 (1984), and private communication.
[46]B. Blankleider and I. R. Afnan, Phys. Rev. C **31**, 1380 (1985).
[47]I. R. Afnan, private communication.